HIGHER-ORDER DGFEM TRANSPORT CALCULATIONS ON POLYTOPE MESHES FOR MASSIVELY-PARALLEL ARCHITECTURES

A Dissertation

by

MICHAEL WAYNE HACKEMACK

Submitted to the Office of Graduate and Professional Studies of
Texas A&M University
in partial fulfillment of the requirements for the degree of

DOCTOR OF PHILOSOPHY

Chair of Committee,	Jean Ragusa
Committee Members,	Marvin Adams
	Jim Morel
	Nancy Amato
	Troy Becker
Head of Department,	Yassin Hassan

August 2016

Major Subject: Nuclear Engineering

1. FEM BASIS FUNCTIONS FOR UNSTRUCTURED POLYTOPES

In Section ??, we detailed the spatial discretization of the transport equation. We then proceeded to give the functional forms for the various elementary matrices needed to form the full set of spatially-discretized PDEs. These included the mass, streaming, and surface matrices where the integrations on the element's domain and boundary require combinations of the basis functions' values and gradients. From FEM theory [1], the basis functions act as interpolation functions with local measure on some subset of elements on a discretized mesh, $\mathbb{T}_h$. To achieve the maximum possible solution convergence rate from Section ?? of $p+1$, the interpolation functions must have polynomial completeness of at least order p. For 2D interpolants, the basis functions are linearly-complete ($p = 1$) if they can exactly interpolate the $\{1, x, y\}$ span of functions. Likewise, 2D basis functions are said to be quadratically-complete if they can exactly interpolate the $\{1, x, y, x^2, xy, y^2\}$ span of functions.

The remainder of the this chapter is organized as follows. In Section 1.1, we present the 2D, linearly-complete, barycentric, polygonal basis functions that we will analyze in this dissertation. We then present in Section ?? the methodology to convert the barycentric polygonal basis functions presented in Section 1.1 into a serendipity space of basis functions with quadratic-completeness. Section ?? provides the methodology that will be employed to generate spatial quadrature sets on 2D arbitrary polygons. Section ?? then presentes the 3D, linearly-complete, polyhedral basis functions that will be exclusively used in Chapter ?? for 3D DSA calculations. We then present numerical results pertaining to our linear and quadratic 2D basis functions in Section ??. Section ?? concludes with some closing remarks.

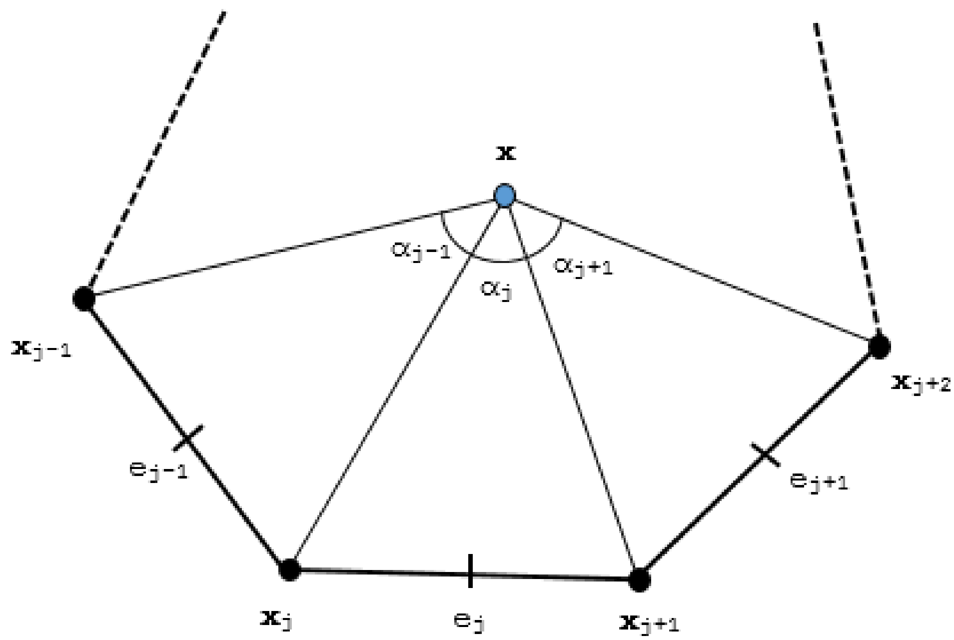

Figure 1.1: Arbitrary polygon with geometric properties used for 2D basis function generation.

1.1 Linear Basis Functions on 2D Polygons

Figure 1.1, gives an image of a reference polygon along with the geometric notations we will use to define the different linear polygonal coordinates. An element, $K \in \mathbb{R}^2$, is defined by a closed set of N_K points (vertices) in $\mathbb{R}^2$. The vertices are ordered $(1, ..., N_K)$ in a counter-clockwise manner without restriction on their convexity. Face j on the polygon, e_j, is defined as the line segment between vertices j and $j+1$. The vertex $j+1$ is determined in general as $j+1 = \mod(j, N_K) + 1$, which gives a wrap-around definition of vertex $N_K + 1 = 1$.

We complete our geometric description for the polygonal coordinate system by analyzing a point $\vec{x}$ inside the polygon's domain, as also seen in Figure 1.1. α_j is the angle between the points $(\vec{x}_j, \vec{x}, \vec{x}_{j+1})$. Since element K is defined by a closed set of $\mathbb{R}^2$ points, α_j is strongly bounded: $([0, \pi])$. We conclude by defining $|\vec{u}|$ as the

Euclidean distance of the vector $\vec{u}$. This means that $|\vec{x} - \vec{x}_j|$ is the distance between the points $\vec{x}$ and $\vec{x}_j$ and $|e_j|$ is the length of face j between points $\vec{x}_j$ and $\vec{x}_{j+1}$.

In this dissertation, all linearly-complete, 2D basis functions for an element K will obey the properties for barycentric coordinates. If the element K is composed of N_K vertices, then it contains N_K barycentric coordinates, where each one is located at a vertex. These barycentric coordinates will form a *partition of unity*,

$$\sum_{j=1}^{N_K} b_j(\vec{x}) = 1; \tag{1.1}$$

coordinate interpolation will result from an *affine combination* of the vertices,

$$\sum_{j=1}^{N_K} b_j(\vec{x})\vec{x}_j = \vec{x}; \tag{1.2}$$

and they will satisfy the *Lagrange property*,

$$b_j(\vec{x}_i) = \delta_{ij}. \tag{1.3}$$

They also have piecewise linearity on faces adjacent to their vertex. As an example of this, consider the coordiantes at vertex j, b_j, along face e_j. Then the piecewise linearity of the coordinate on the face means that it can interpolate as

$$b_j((1-\mu)\vec{x}_j + \mu\vec{x}_{j+1}) = (1-\mu)b_j(\vec{x}_j) + \mu b_j(\vec{x}_{j+1}), \qquad \mu \in [0,1]. \tag{1.4}$$

Using the *partition of unity* of Eq. (1.1), we can rewrite Eqs. (1.1-1.2) into a separate, compact, vectorized form for completeness

$$\sum_{j=1}^{N_K} b_j(\vec{x})\vec{c}_{j,1}(\vec{x}) = \vec{q}_1, \tag{1.5}$$

where $\vec{c}_{j,1}(\vec{x})$ and $\vec{q}_1$ are the lineary-complete constraint and equivalence terms, respectively. These terms are simply:

$$\vec{c}_{j,1}(\vec{x}) = \begin{bmatrix} 1 \\ x_j - x \\ y_j - y \end{bmatrix} \quad \text{and} \quad \vec{q}_1 = \begin{bmatrix} 1 \\ 0 \\ 0 \end{bmatrix}, \tag{1.6}$$

respectively. Equation (1.5) states that our interpolation functions (the basis functions) can exactly reproduce polynomial functions up to order 1. This is why we state that our basis functions are linearly-complete. However, we will not restrict our N_K basis functions to be polynomials. In fact, of the basis functions that we will use, only the PWL coordinates are formed by combinations of polynomial functions.

1.1.1 Wachspress Rational Basis Functions

The first linearly-complete polygonal coordinates that we will consider are the Wachspress rational functions [2]. These rational functions were the first derived for 2D polygons and possess all the properties of the barycentric coordinates previously detailed. However, they are only valid interpolants over strictly-convex polygons. They have zero measure and blow up for weakly-convex and concave polygons, respectively. Also, their values and gradients cannot be directly evaluated on the polygonal boundary. However, they do have a valid limit which we show in Appendix **??**. The Wachspress coordinates (which we denote as b^W) have the following form

$$b_j^W(\vec{x}) = \frac{w_j(\vec{x})}{\sum_i w_i(\vec{x})}, \tag{1.7}$$

where the Wachspress weight function for vertex j, w_j, has the following definition:

$$w_j(\vec{x}) = \frac{A(\vec{x}_{j-1}, \vec{x}_j, \vec{x}_{j+1})}{A(\vec{x}, \vec{x}_{j-1}, \vec{x}_j)\, A(\vec{x}, \vec{x}_j, \vec{x}_{j+1})}. \tag{1.8}$$

In Eq. (1.8), the terms $A(\vec{a}, \vec{b}, \vec{c})$ denote the signed area of the triangle with vertices $\vec{a}$, $\vec{b}$, and $\vec{c}$. Each of these signed areas can be computed by

$$A(\vec{a}, \vec{b}, \vec{c}) = \frac{1}{2} \begin{vmatrix} 1 & 1 & 1 \\ x_a & x_b & x_c \\ y_a & y_b & y_c \end{vmatrix}. \tag{1.9}$$

There is an alternative method of expressing the Wachspress weight functions. Warren et al. [3] proposed weight functions that are defined in terms of the perpindicular distance of the point $\vec{x}$ to the polygon's faces. Using the reference polygon of Figure 1.1, the perpendicular distance of the point $\vec{x}$ to the face j is denoted as $h_j(\vec{x})$ and is given by

$$h_j(\vec{x}) = \left(\vec{x}_j - \vec{x}\right) \cdot \vec{n}_j = \left(\vec{x}_{j+1} - \vec{x}\right) \cdot \vec{n}_j, \tag{1.10}$$

where $\vec{n}_j$ is the outward normal direction of face j. Using these perpdendicular distance, the Wachspress coordinates can be calculated using Eq. (1.7) with new function definitions of

$$w_j(\vec{x}) = \frac{\vec{n}_{j-1} \,\mathrm{x}\, \vec{n}_j}{h_{j-1}(\vec{x}) h_j(\vec{x})}, \tag{1.11}$$

where

$$\vec{x}_1 \,\mathrm{x}\, \vec{x}_2 = \begin{vmatrix} x_1 & x_2 \\ y_1 & y_2 \end{vmatrix}. \tag{1.12}$$

For FEM theory, the basis function gradients are also necessary to compute some of the elementary matrices. The gradients of the Wachspress rational functions are straightforward to calculate by simply taking the partial derivatives of Eq. (1.7). Then, using derivative rules along with some algebra, the Wachspress gradients are given by,

$$\vec{\nabla} b_j^W(\vec{x}) = b_j^W(\vec{x}) \left(\vec{R}_j(\vec{x}) - \sum_i b_i^W(\vec{x}) \vec{R}_i(\vec{x}) \right), \tag{1.13}$$

where the reduced gradient, $\vec{R}_i$, is defined as

$$\vec{R}_i(\vec{x}) = \frac{1}{w_i} \vec{\nabla} w_i. \tag{1.14}$$

This means that the gradients of the Wachspress coordinates can be calculated by combinations of the all the weight functions and their gradients. The weight function gradients are easy to compute using the perpendicular form. The gradient of the j weight functions is given by

$$\vec{\nabla} w_j(\vec{x}) = w_j(\vec{x}) \left(\frac{\vec{n}_{j-1}}{h_{j-1}(\vec{x})} + \frac{\vec{n}_j}{h_j(\vec{x})} \right). \tag{1.15}$$

This lets us immediately see that $\vec{R}_j$ is simply

$$\vec{R}_i(\vec{x}) = \frac{\vec{n}_{j-1}}{h_{j-1}(\vec{x})} + \frac{\vec{n}_j}{h_j(\vec{x})}. \tag{1.16}$$

We now give a pair of contour plots of the Wachspress coordinates. First, Figure 1.2 provides the contour plots of the four Wachspress functions on the unit square. We see that the functions are smoothly varying within the square with at least C^1 continuity. Then in Figure 1.3, we give the contour plots for a degenerate pentagon

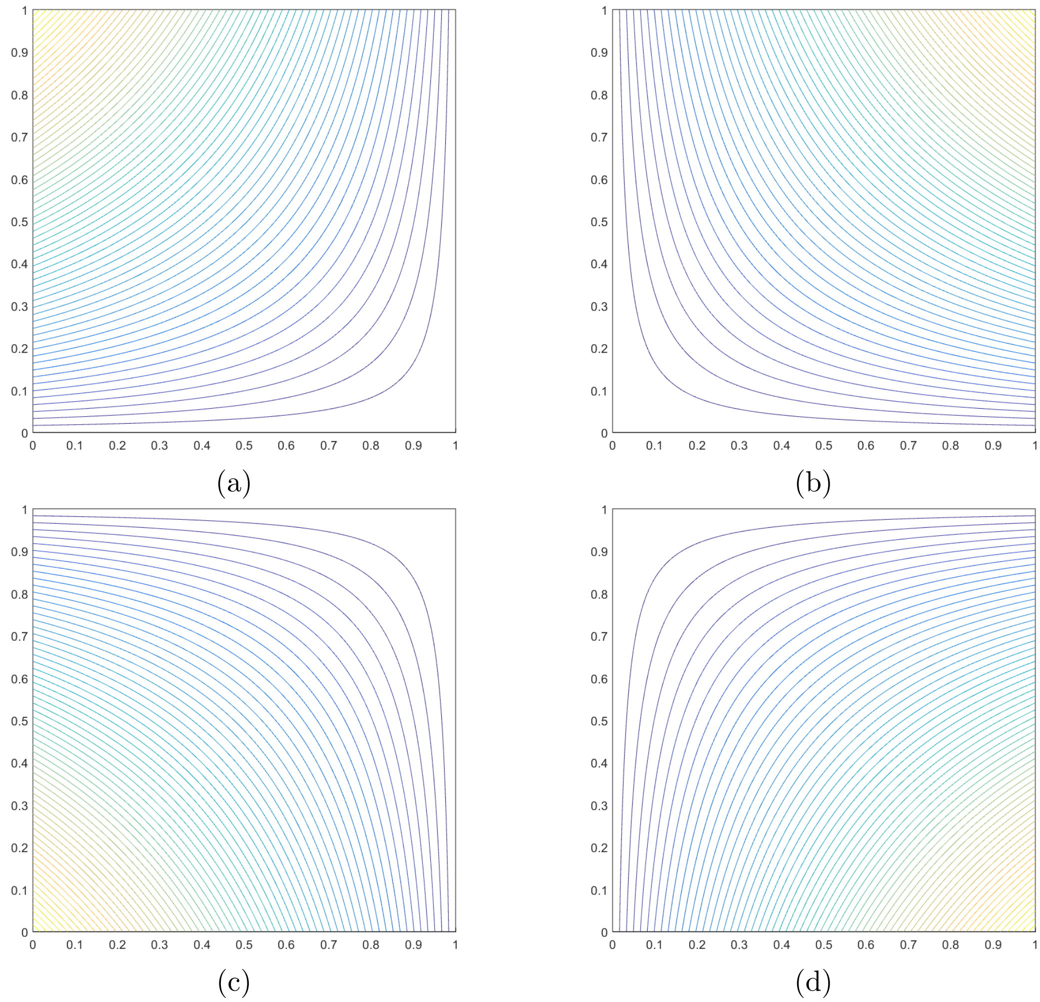

Figure 1.2: Contour plots of the linear Wachspress basis functions on the unit square for the vertices located at: (a) (0,1), (b) (1,1), (c) (0,0), and (d) (1,0).

which is simply the unit square with a vertex added at point $(1/2, 1)$. We see how the functions fail for this weakly-convex case. The function located at the degenerate vertex has zero measure everywhere within the polygon. Also, the functions located at the vertices adjacent to the degenerate vertex no longer maintain linearity on their adjacent faces. We will not show it here for brevity, but the Wachspress functions on concave polygons will have points in the interior that will result in divide-by-zero operations.

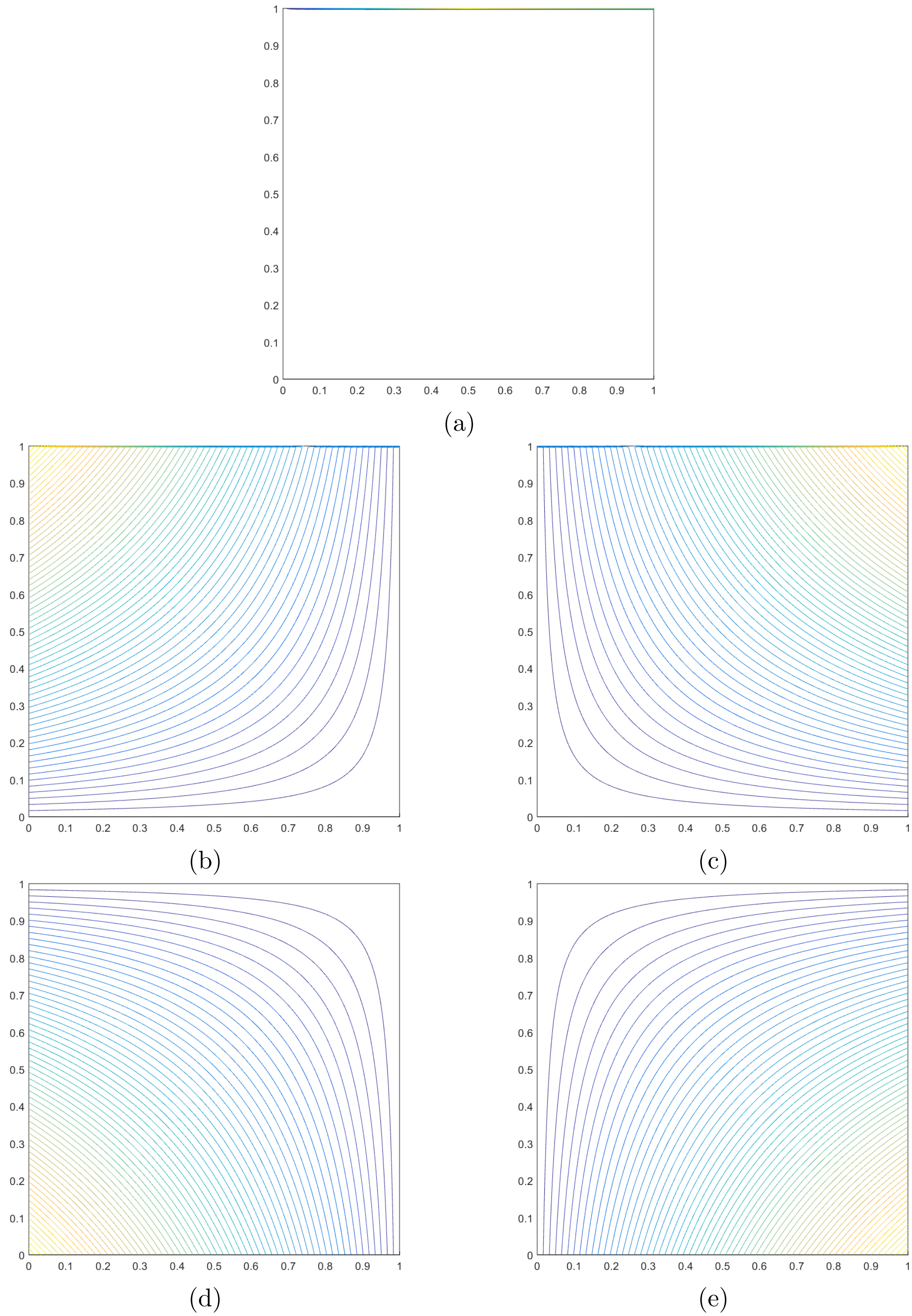

Figure 1.3: Contour plots of the linear Wachspress basis functions on the degenerate pentagon for the vertices located at: (a) (1/2,1), (b) (0,1), (c) (1,1), (d) (0,0), and (e) (1,0).

1.1.2 Piecewise Linear (PWL) Basis Functions

The second linearly-complete 2D polygonal coordinates that we will analyze are the Piecewise Linear (PWL) coordinates proposed by Stone and Adams [4, 5]. They originally introduced the PWL coordinates to work specifically for the DGFEM transport equation on unstructured quadrilateral and polygonal grids. These coordinates share some similarities with the Wachspress rational functions, but also contain some key differences. The properties of the PWL coordinates that are different from the Wachspress rational functions can be summarized with the following:

1. PWL works with concave polytopes;
2. PWL cannot interpolate on curved surfaces;
3. points on the boundary can be directly evaluated;
4. the PWL integrals can be computed analytically;
5. the PWL functions are only C^0 continuous: their gradients are discontinuous within the element.

The 2D PWL functions are defined as combinations of linear triangular functions, with some of them only having measure within a subregion of a polygon. These subregions are formed by triangulating the arbitrary 2D polygon into a set of sub-triangles. Each sub-triangle is defined by two adjacent vertices (taken in a counter-clockwise ordering to maintain consistency) and the polygon's centroid, $\vec{r}_c$. Looking at Figure 1.1 as an example, sub-triangle j is defined by the points $\{\vec{x}_j, \vec{x}_{j+1}, \vec{r}_c\}$, which are the polygon's vertices j and $j+1$ and the polygon's centroid. If a polygon K has N_K vertices, then its centroid can be defined by

$$\vec{r}_c = \sum_{j=1}^{N_K} \alpha_j^K \vec{x}_j, \tag{1.17}$$

where α_j^K are the vertex weights functions and,

$$\sum_{j=1}^{N_K} \alpha_j^K = 1. \tag{1.18}$$

For this work, we continue to use the definition for the vertex weight functions from previous works [4, 5, 6],

$$\alpha_j^K = \frac{1}{N_K}. \tag{1.19}$$

This means that the weight functions are equal for every vertex and the cell centroid simply becomes the average position of all the vertices. However, we note that care must be taken so that the centroid does not like on the polygon's boundary. This will cause the PWL functions to no longer have piecewise linearity along the boundary. Using these vertex weight functions, the PWL basis function for vertex j, b_j^{PWL}, is defined as

$$b_j^{PWL}(x, y) = t_j(x, y) + \alpha_j^K t_c(x, y). \tag{1.20}$$

In Eq. (1.20), t_j is the standard 2D linear function with unity at vertex j that linearly decreases to zero to the cell center and each adjoining vertex. t_c is the 2D cell "tent" function located at $\vec{r}_c$ which is unity at the cell center and linearly decreases to zero to each cell vertex. α_j^K is the weight parameter for vertex j in cell K. The functional form of Eq. (1.20) with constant vertex weights means that the PWL function for vertex j, within the domain of K, linearly decreases to a value of $1/N_K$ at the polygonal center. From there, the function linearly decreases to zero on all faces that are not connected to vertex j. The gradients of the PWL functions are easy to compute term-by-term in a straightforward manner:

$$\vec{\nabla} b_j^{PWL}(x,y) = \vec{\nabla} t_j(x,y) + \alpha_j^K \vec{\nabla} t_c(x,y). \tag{1.21}$$

We now give some example contour plots of the PWL coordinates over different polygons. First, we provide the contour plots for the four PWL functions on the unit square in Figure 1.4. In this example it is easy to discern the functional form of Eq. (1.20) with the use of constant vertex weights. We clearly see each function linearly decrease from its vertex to the cell center (with a value of $1/N_K$) and then linearly decrease to all non-adjoining faces. Next, Figure 1.5 provides the contour plots for the PWL functions on a degenerate (weakly-convex) pentagon where a fifth vertex was added to the unit square at $(1/2, 1)$. Unlike the Wachspress coordinates, the PWL functions work on weakly-convex polygons. The final example we give in Figure 1.6 is a favorite in the applied mathematics community: the “L-shaped” domain. It provides an example of PWL's ability to still be linearly-complete on concave polygons. In this example, the cell centroid was forced to be at the point $(1/3, 1/3)$ so that it would be inside of the polygon.

1.1.3 Mean Value Basis Functions

At this point, we now introduce the first new polygonal basis set for use with the transport equation: the *mean value coordinates* (MV) developed by Floater [7, 8]. The original motivation behind the MV coordinates was to approximate harmonic maps on a polygon by a set of piecewise linear maps over a triangulation of the polygon for use in computer aided graphic design.

$$\nabla^2 u = 0, \tag{1.22}$$

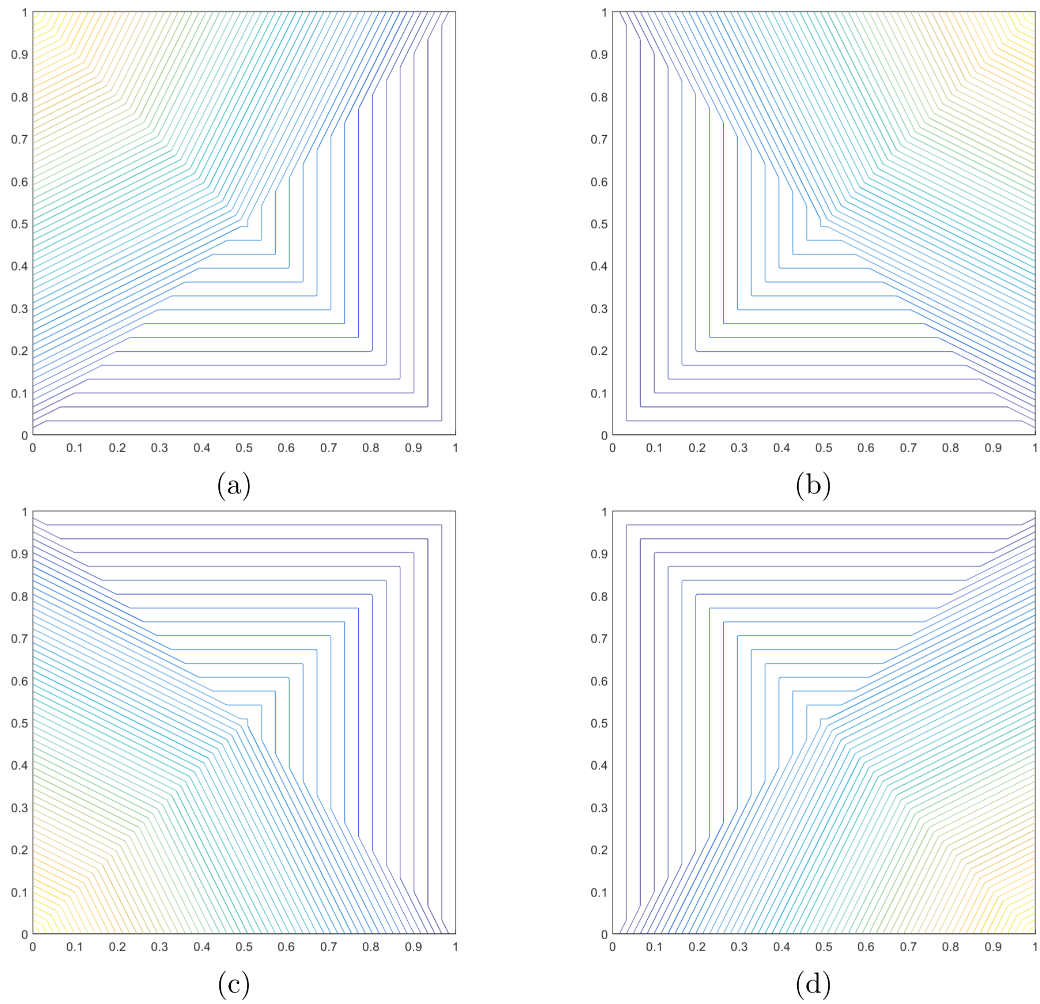

Figure 1.4: Contour plots of the linear PWL basis functions on the unit square for the vertices located at: (a) (0,1), (b) (1,1), (c) (0,0), and (d) (1,0).

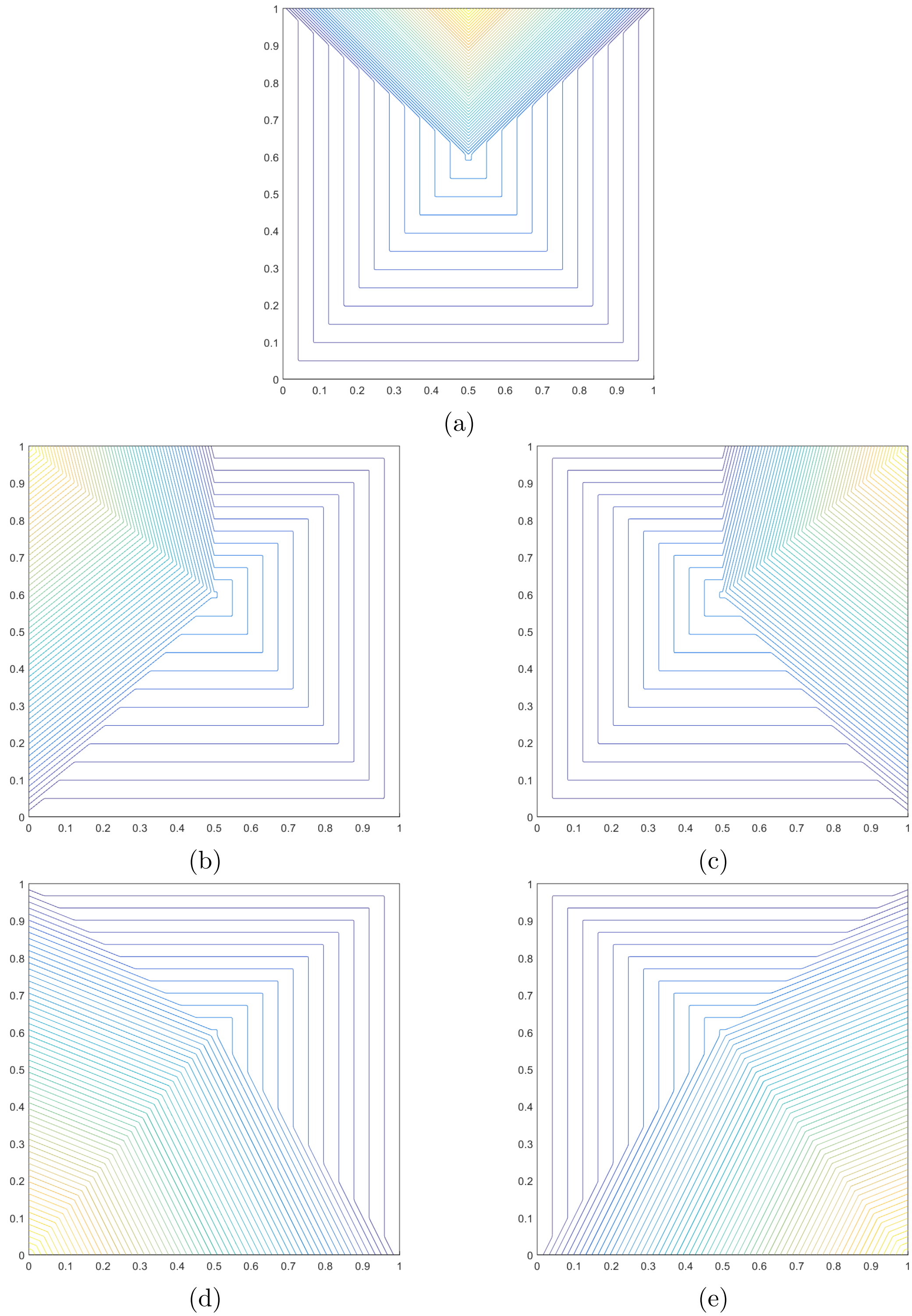

Figure 1.5: Contour plots of the linear PWL basis functions on the degnerate pentagon for the vertices located at: (a) (1/2,1), (b) (0,1), (c) (1,1), (d) (0,0), and (e) (1,0).

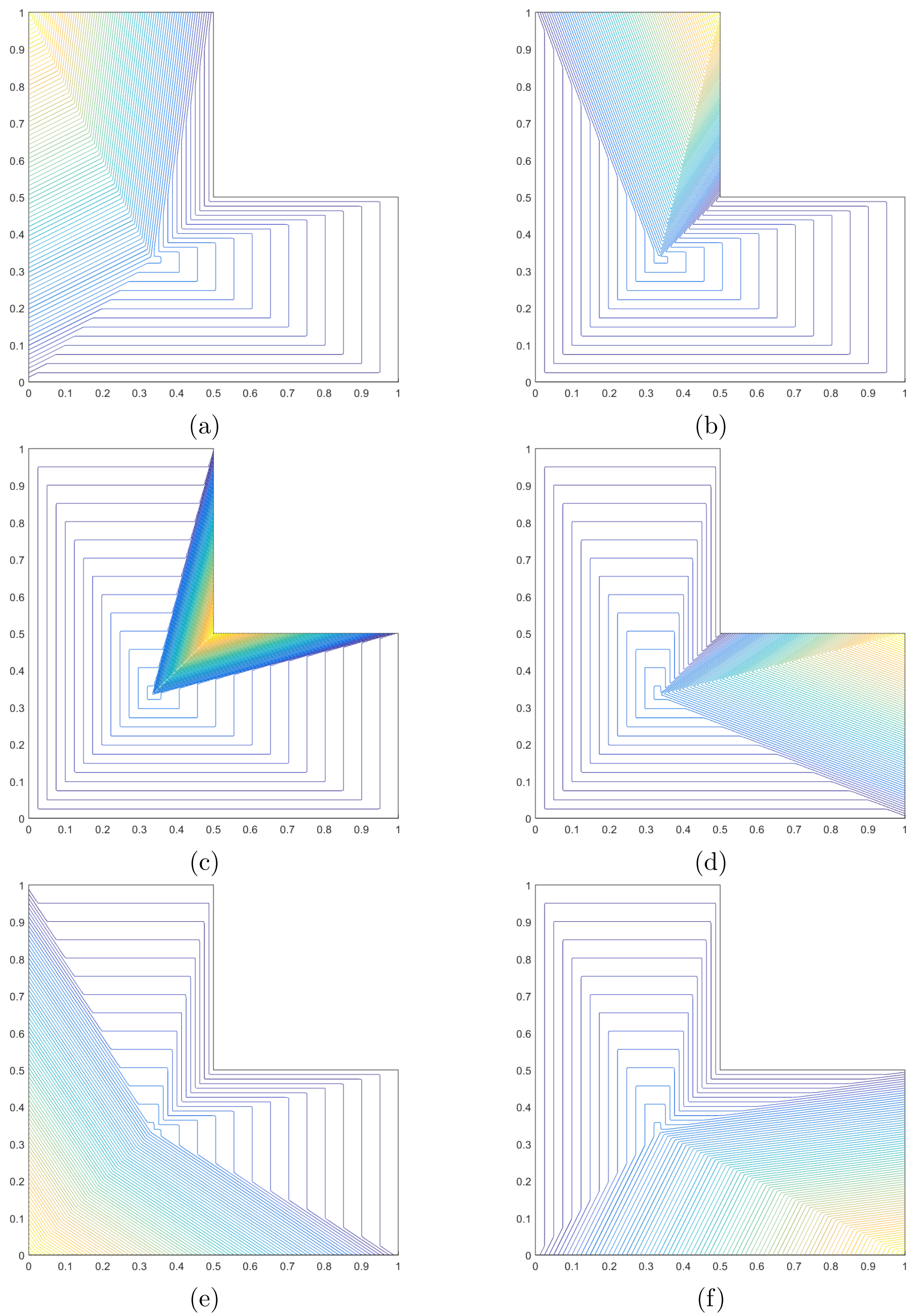

Figure 1.6: Contour plots of the linear PWL basis functions on the L-shaped domain for the vertices located at: (a) (0,1), (b) (1/2,1), (c) (1/2,1/2), (d) (1,1/2), (e) (0,0), and (f) (1,0).

with $u(\vec{r}) = u_0$ constituting a piecewise linear function

$$b_j^{MV}(\vec{x}) = \frac{w_j(\vec{x})}{\sum_i w_i(\vec{x})} \tag{1.23}$$

where the mean value weight function for vertex j, w_j, has the following definition:

$$w_j(\vec{x}) = \frac{\tan(\alpha_{j-1}/2) + \tan(\alpha_j/2)}{|\vec{x}_j - \vec{x}|} \tag{1.24}$$

$$\vec{\nabla} b_j^{MV}(\vec{x}) = b_j^{MV}(\vec{x}) \left(\vec{R}_j(\vec{x}) - \sum_i b_i^{MV}(\vec{x}) \vec{R}_i(\vec{x}) \right), \tag{1.25}$$

,

and where the reduced gradient, $\vec{R}_j$, still has the same definition from Eq. (1.14). If we define $t_j = \tan(\alpha_j/2)$ and $t_{j-1} = \tan(\alpha_{j-1}/2)$, then after extensive algebra, the mean value reduced gradients are

$$\vec{R}_j = \left(\frac{t_{j-1}}{t_{j-1} + t_j} \right) + \left(\frac{t_j}{t_{j-1} + t_j} \right) + \frac{\vec{g}_j}{|\vec{x}_i - \vec{x}|}, \tag{1.26}$$

where

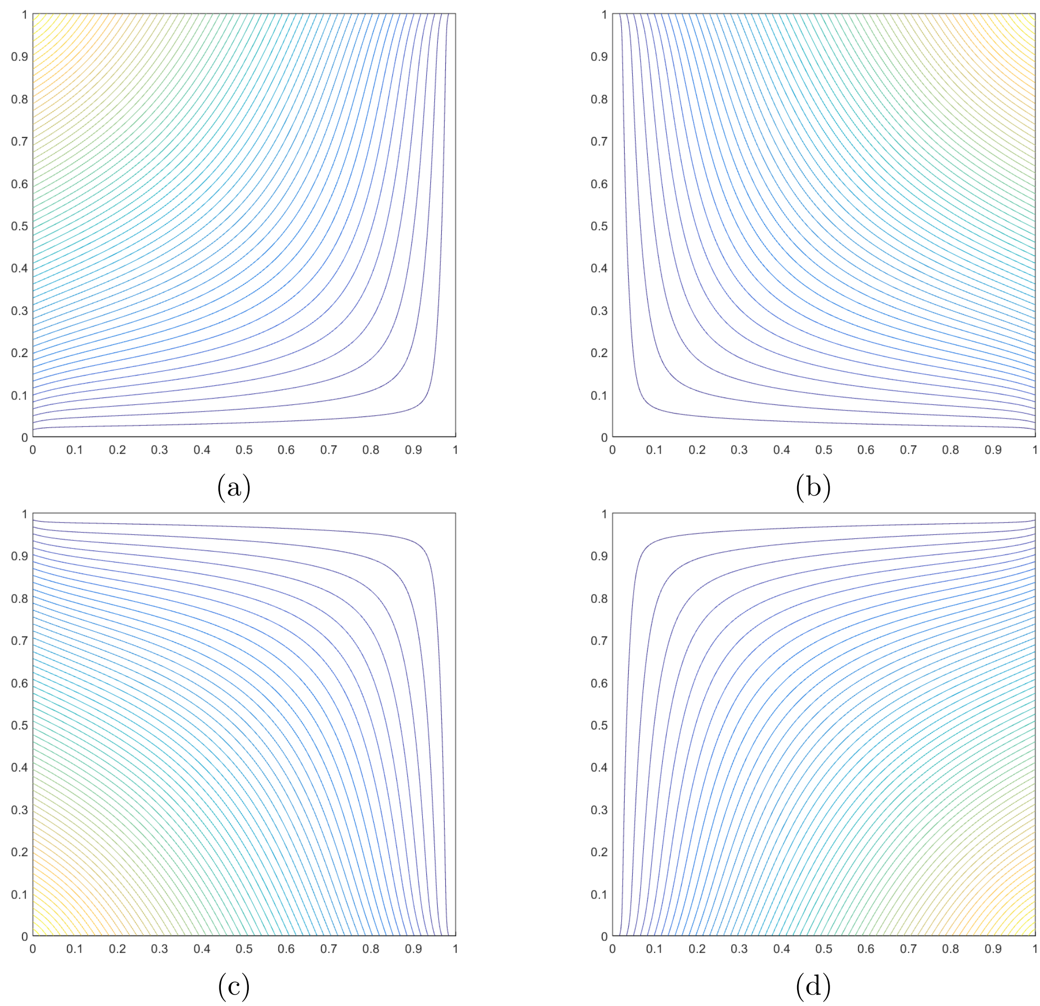

Figure 1.7: Contour plots of the linear mean value basis functions on the unit square for the vertices located at: (a) (0,1), (b) (1,1), (c) (0,0), and (d) (1,0).

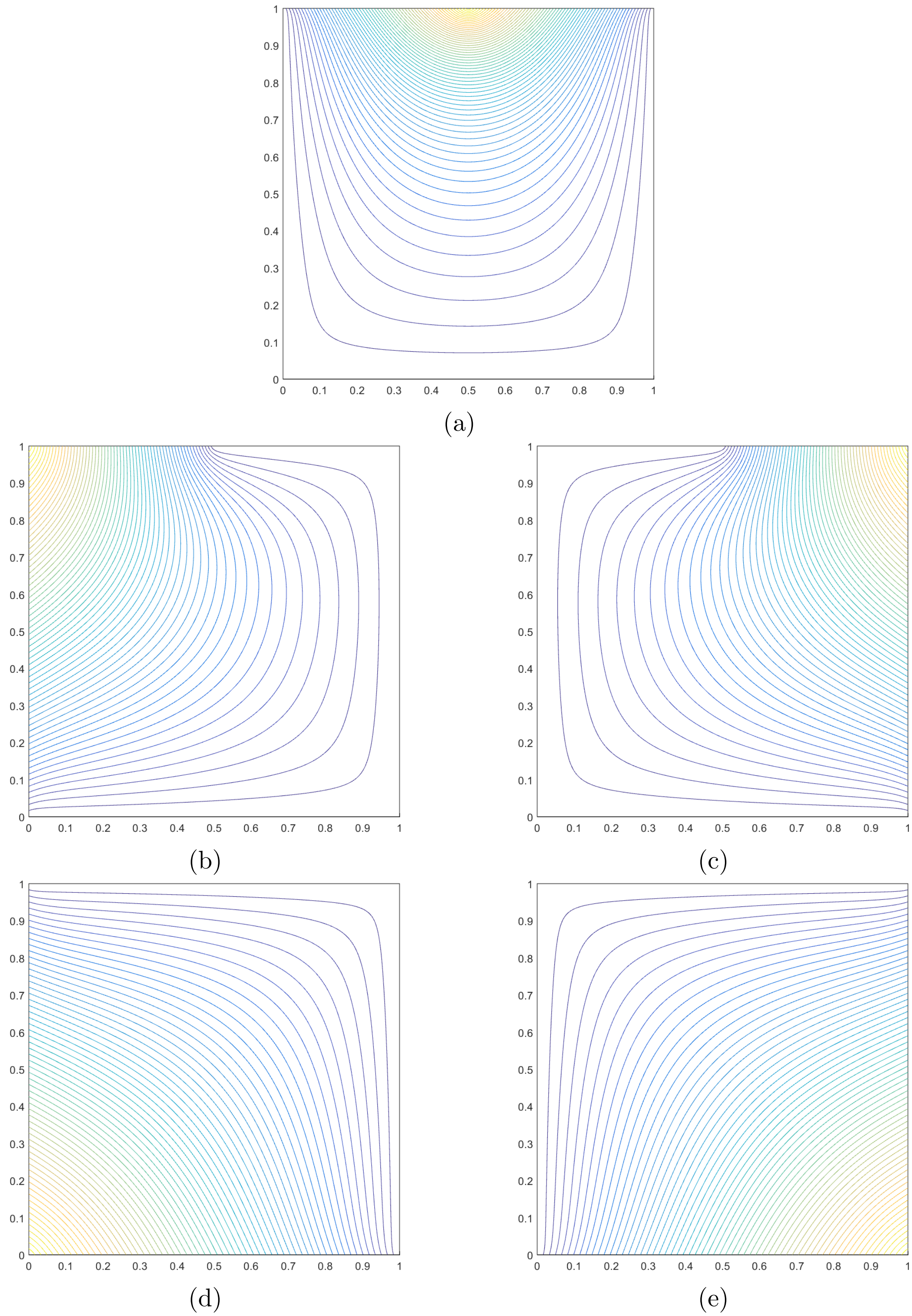

Figure 1.8: Contour plots of the linear mean value basis functions on the degenerate pentagon for the vertices located at: (a) (1/2,1), (b) (0,1), (c) (1,1), (d) (0,0), and (e) (1,0).

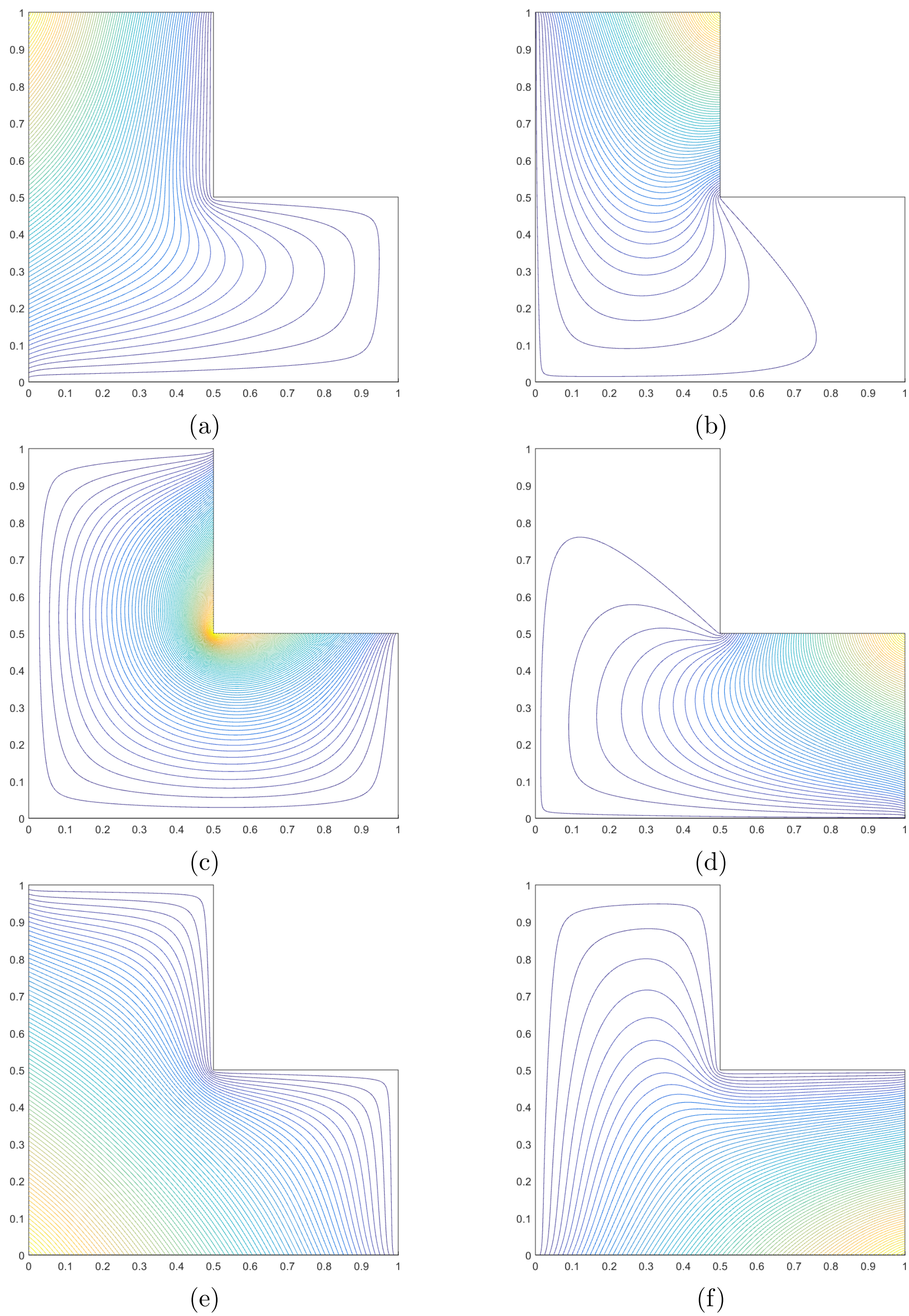

Figure 1.9: Contour plots of the linear mean value basis functions on the L-shaped domain for the vertices located at: (a) (0,1), (b) (1/2,1), (c) (1/2,1/2), (d) (1,1/2), (e) (0,0), and (f) (1,0).

REFERENCES

[1] A. ERN and J.-L. GUERMOND, *Theory and practice of finite elements*, vol. 159, Springer Science & Business Media (2013).

[2] E. L. WACHSPRESS, "A Rational Finite Element Basis," *Mathematics in science and engineering* (1975).

[3] J. WARREN, S. SCHAEFER, A. N. HIRANI, and M. DESBRUN, "Barycentric coordinates for convex sets," *Advances in computational mathematics*, **27**, *3*, 319–338 (2007).

[4] H. G. STONE and M. L. ADAMS, "A piecewise linear finite element basis with application to particle transport," in "Proc. ANS Topical Meeting Nuclear Mathematical and Computational Sciences Meeting," (2003).

[5] H. G. STONE and M. L. ADAMS, "New Spatial Discretization Methods for Transport on Unstructured Grids," in "Proc. ANS Topical Meeting Mathematics and Computation, Supercomputing, Reactor Physics and Biological Applications," (2005).

[6] T. S. BAILEY, *The piecewise linear discontinuous finite element method applied to the RZ and XYZ transport equations*, Ph.D. thesis, Texas A&M University (2008).

[7] M. S. FLOATER, "Mean value coordinates," *Computer aided geometric design*, **20**, *1*, 19–27 (2003).

[8] K. HORMANN and M. S. FLOATER, "Mean value coordinates for arbitrary planar polygons," *ACM Transactions on Graphics (TOG)*, **25**, *4*, 1424–1441 (2006).